Report

Cell Reports

DUX4-Induced Histone Variants H3.X and H3.Y Mark DUX4 Target Genes for Expression

Graphical Abstract

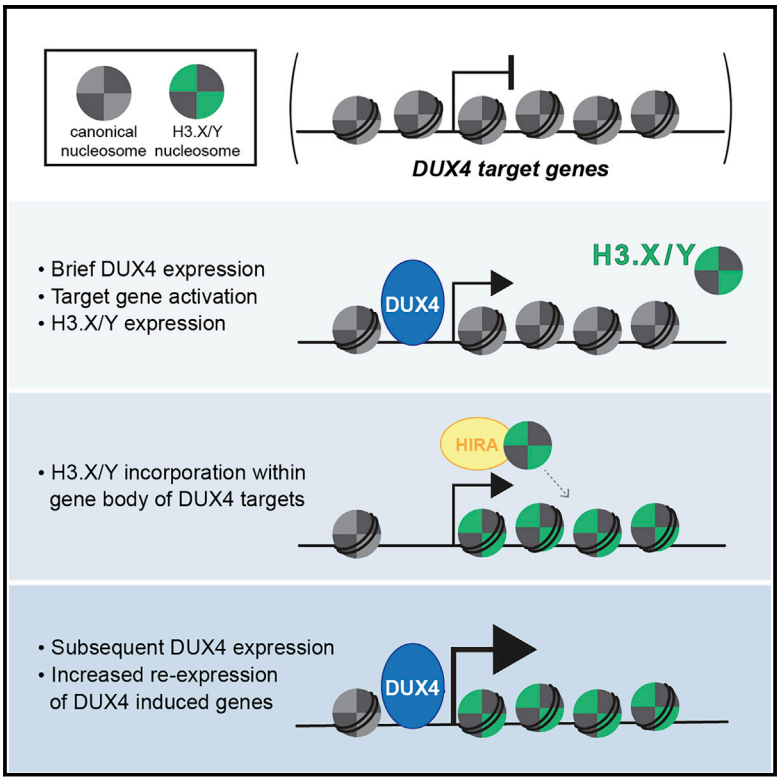

Highlights

- The cleavage-stage transcription factor DUX4 induces histone variants H3.X and H3.Y
- H3.X/Y incorporate into genes transcriptionally induced by DUX4
- H3.X/Y incorporation results in enhanced re-activation of DUX4-regulated genes
- H3.X/Y are necessary to amplify the DUX4 network in FSHD muscle cells

Authors

Rebecca Resnick, Chao-Jen Wong, Danielle C. Hamm, ..., Steven Henikoff, Silvère M. van der Maarel, Stephen J. Tapscott

Correspondence

stapscot@fredhutch.org

In Brief

Resnick et al. show that the DUX4-induced histone variants, H3.X and H3.Y, incorporate into the chromatin of DUX4-induced genes, making them more sensitive to subsequent expression. This suggests a mechanism for how the brief expression of DUX4 can establish a memory of its transcriptional network.

Resnick et al., 2019, Cell Reports *29*, 1812–1820
November 12, 2019
https://doi.org/10.1016/j.celrep.2019.10.025

CellPress

OPEN ACCESS
CellPress

Cell Reports
Report

DUX4-Induced Histone Variants H3.X and H3.Y Mark DUX4 Target Genes for Expression

Rebecca Resnick,[1,2,3] Chao-Jen Wong,[1] Danielle C. Hamm,[1] Sean R. Bennett,[1] Peter J. Skene,[4] Sandra B. Hake,[5] Steven Henikoff,[6] Silvère M. van der Maarel,[7] and Stephen J. Tapscott[1,8,*]

[1]Human Biology Division, Fred Hutchinson Cancer Research Center, Seattle, WA 98109, USA
[2]Molecular and Cellular Biology Program, University of Washington, Seattle, WA 98195, USA
[3]Medical Scientist Training Program, University of Washington, Seattle, WA 98195, USA
[4]NanoString Technologies, Seattle, WA 98109, USA
[5]Institute for Genetics, Justus-Liebig-University Giessen, Hessen, Germany
[6]Basic Science Division, Fred Hutchinson Cancer Center, Seattle, WA 98109, USA
[7]Department of Human Genetics, Leiden University Medical Center, 2333 Leiden, the Netherlands
[8]Lead Contact
*Correspondence: stapscot@fredhutch.org
https://doi.org/10.1016/j.celrep.2019.10.025

SUMMARY

The DUX4 transcription factor is briefly expressed in the early cleavage-stage embryo, where it induces an early wave of zygotic gene transcription, whereas its mis-expression in skeletal muscle causes the muscular dystrophy facioscapulohumeral dystrophy (FSHD). Here, we show that DUX4 induces the expression of the histone variants *H3.X* and *H3.Y*. We have used a myoblast cell line with doxycycline-inducible DUX4 to show that these histone variants are incorporated throughout the body of DUX4-induced genes. Following a brief pulse of DUX4, these histones contribute to greater perdurance and to enhanced re-activation of DUX4 target gene expression. These findings provide a model for H3.X/Y as a chromatin mechanism that facilitates the expression of DUX4 target genes subsequent to a brief pulse of DUX4 expression.

INTRODUCTION

Mis-expression of the double homeobox transcription factor *DUX4* in skeletal muscle is the cause of facioscapulohumeral muscular dystrophy (FSHD) (Tawil et al., 2014). In cultured FSHD muscle cells, there is a de-repression of the *DUX4* retrogene, resulting in a burst of *DUX4* expression from a minority of myonuclei. In contrast to the toxicity of *DUX4* expression in skeletal muscle cells, *DUX4* is normally expressed in the early cleavage-stage embryo, where it regulates zygotic genome activation (De Iaco et al., 2017; Hendrickson et al., 2017; Whiddon et al., 2017). In both of these cases, the burst expression of *DUX4* results in a perdurant developmental or pathological phenotype. This could be due to the initiation of a transcription factor cascade, an induced chromatin memory, or both.

Histone variants play critical roles in early development, such as the recently demonstrated requirement for *H3.3* in paternal genome activation in mouse preimplantation embryos (Kong et al., 2018) as well as for retroelement silencing in embryonic stem cells (Elsässer et al., 2015). Although canonical H3 is incorporated into newly synthesized DNA, H3.3 and H3.3 variants are made throughout the cell cycle (Ahmad and Henikoff, 2002a) and use either the ATRX/DAXX complex to incorporate into repressed regions (Drané et al., 2010; Goldberg et al., 2010; Lewis et al., 2010) or the HIRA chaperone to incorporate into transcriptionally active DNA (Ahmad and Henikoff, 2002b; Tagami et al., 2004). Canonical H3 and H3.3 are extremely well conserved and differ by only 4 to 5 amino acids. More divergent histone variants, such as CENP-A and H3t, have more specialized roles in designating centromeres or facilitating the transition from histones to protamines during spermiogenesis, respectively (Howman et al., 2000; Tachiwana et al., 2010).

Histone variants *H3.X* and *H3.Y* were recently identified in the human genome as a multicopy gene family interspersed with the *TAF11-like* macrosatellite repeat (Wiedemann et al., 2010). Biochemical studies of H3.Y nucleosomes showed that they resulted in a more relaxed chromatin configuration than H3.3 nucleosomes, excluded linker histone H1, were incorporated at transcriptional start sites (TSSs) of actively transcribed genes, and that H3.Y used the HIRA chaperone (Kujirai et al., 2016; Zink et al., 2017). Collectively, these data suggest that H3.Y, and possibly H3.X as well, might be incorporated at active genes and help to maintain an open chromatin conformation.

Here, we show that DUX4 induces the expression of *H3.X* and *H3.Y* and that these histone variants are incorporated in highly transcribed DUX4 target genes. A short pulse of *DUX4* that mimics its developmental expression pattern induced *H3.X/Y* expression and the majority of DUX4-regulated genes but was not cytotoxic, permitting the analysis of longer term consequences of DUX4 expression. DUX4-induced expression of *H3.X/Y* resulted in greater perdurance of DUX4 target gene expression and enhanced activation with a second pulse of *DUX4*. Together, these results indicate that incorporation of H3.X/Y at DUX4-induced genes contributes to prolonged expression and sensitizes these genes to subsequent induction.

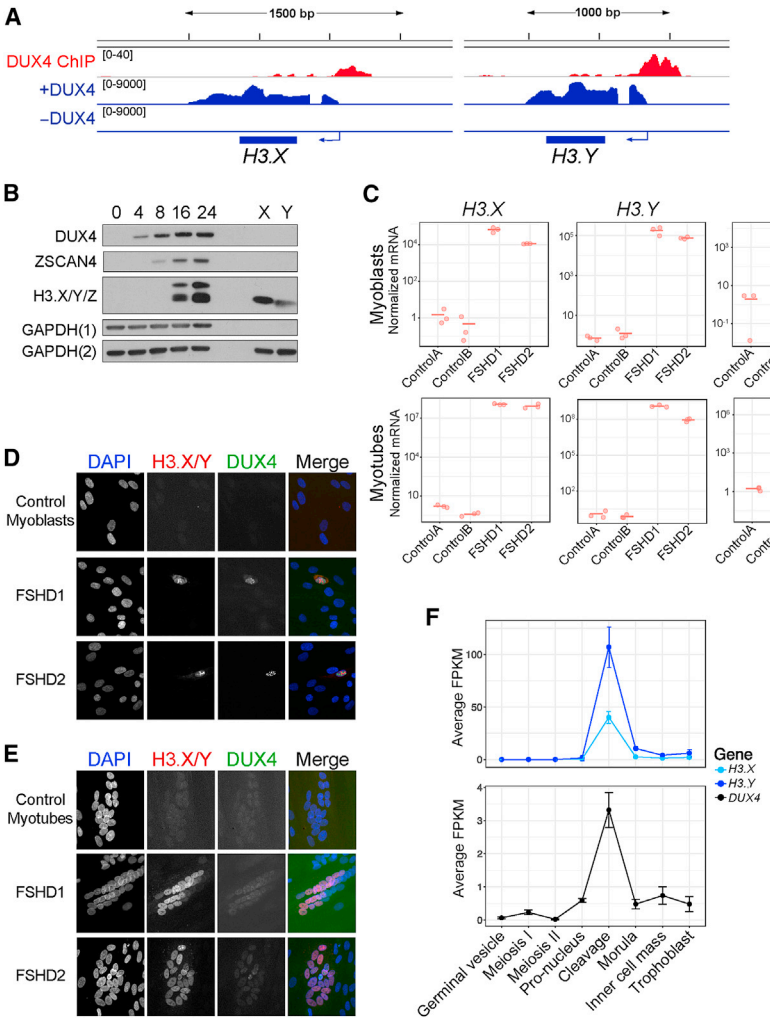

Figure 1. DUX4 Induces the Expression of Histone Variants *H3.X* and *H3.Y*

(A) RNA-seq (blue) and ChIP-seq (red) tracks from Jagannathan et al. (2016) and Geng et al. (2012), respectively, showing that *H3.X* and *H3.Y* were induced with *DUX4* induction and that DUX4 was bound upstream of *H3.X* and *H3.Y*.

(B) Western blot analysis of MB135iDUX4 time course after *DUX4* induction. H3.X and H3.Y migrate at slightly different sizes as shown by *in vitro* translated protein (lanes X and Y). The larger band corresponds to the predicted size for H3.Z. GAPDH(1) and GAPDH(2) represent loading controls for DUX4 or ZSCAN4 and H3.X/Y/Z, respectively.

(C) qRT-PCR analysis of *DUX4*, *H3.X*, and *H3.Y* in control, FSHD1, and FSHD2 myoblasts and myotubes performed in biological triplicates. Values were normalized to the average of the control samples. ControlA = 54-1, ControlB = MB135, FSHD1 = 54-2, and FSHD2 = MB200.

(D and E) Immunofluorescence of H3.X/Y (red) and DUX4 (green) in FSHD1, FSHD2, and control myoblasts and myotubes.

(E) DUX4 and H3.X/Y co-stain rare FSHD myoblast cells and nuclei within myotubes, with no staining seen in control cells. DAPI channel in myoblasts and H3.X/Y and DUX4 channels in myotubes were brightened equally for all samples.

(F) Average fragments per kilobase of transcript per million mapped reads (FPKM) of reads from indicated stages of early human embryos (Hendrickson et al., 2017) that map to *H3.X*, *H3.Y*, and *DUX4*. Expression data displayed as mean with standard deviation of replicates.

See also Figure S1.

RESULTS

DUX4 Induces the Expression of Histone Variants *H3.X* and *H3.Y*

To study the transcriptional network activated by DUX4, we have used a well-characterized cellular model system of human myoblasts with a doxycycline-inducible *DUX4* transgene (MB135iDUX4 cells; Jagannathan et al., 2016). Induction of *DUX4* in these cells has been shown to induce many DUX4-regulated genes belonging to the transcriptional program characteristic of the early cleavage-stage embryo (Hendrickson et al., 2017; Whiddon et al., 2017) and recapitulates the transcriptional consequences of endogenous *DUX4* expression in FSHD cells (Jagannathan et al., 2016; Yao et al., 2014). As such, it is a validated model system for the identification of DUX4-regulated genes and the biological consequences of *DUX4* expression.

Further analysis of our previous RNA sequencing datasets (Jagannathan et al., 2016) revealed high expression of unannotated transcripts in the region of the *TAF11-like* macrosatellite repeat array on chromosome 5 that were not detected in the absence of *DUX4* induction. Some of these sequences correspond to histone variants *H3.X* and *H3.Y* (Wiedemann et al., 2010), as well as a previously unreported related sequence we designated *H3.Z* (Figure S1A). Chromatin immunoprecipitation sequencing (ChIP-seq) (Geng et al., 2012) showed DUX4 binding near the TSS of *H3.X*, *H3.Y*, and *H3.Z* loci (Figures 1A and S1D), suggesting they are direct targets of DUX4. Compared to *H3.X* or *H3.Y*, *H3.Z* has a frameshift mutation that disrupts the histone fold and produces a longer protein (Figures S1A and S1B). Although overexpression of *H3.X* or *H3.Y* in myoblasts resulted in nuclear staining, overexpression of *H3.Z* did not (Figure S1C), suggesting H3.Z does not generate a functional histone protein. Therefore, moving forward, we focused our efforts on the characterization of DUX4-induced expression of *H3.X* and *H3.Y*.

Western analysis with an antibody to an epitope shared by H3.X, H3.Y, and H3.Z (Wiedemann et al., 2010) detected both H3.X and H3.Y between 8 and 16 h after *DUX4* induction in MB135iDUX4 cells, with levels increasing up to 24 h (Figure 1B). H3.X is slightly larger than H3.Y, as shown by *in vitro* translated protein, generating a closely spaced doublet. In addition to H3.X and H3.Y (see lanes labeled X and Y in Figure 1B), a band migrating at the size of H3.Z was also detected.

To determine whether endogenous DUX4 also regulated *H3.X/Y*, we used myoblast cell lines derived from individuals

with FSHD1 and FSHD2, the two forms of the disease (Tawil et al., 2014), which show sporadic de-repression of *DUX4* in ~0.1% of cells (Snider et al., 2010), with increasing frequency and amount of *DUX4* expression upon differentiation to myotubes (Jones et al., 2012; Krom et al., 2012; Snider et al., 2010). qRT-PCR detected elevated levels of *DUX4*, *H3.X*, *H3.Y*, and *H3.Z* in both FSHD1 and FSHD2 myoblast cultures, but not in controls, with increased expression in the FSHD myotubes (Figures 1C and S1E). Immunofluorescence showed strong nuclear H3.X/Y staining in FSHD myoblasts and myotubes, which also co-localized with DUX4 staining, whereas no control myoblasts or myotubes stained positively for either H3.X/Y or DUX4 (Figures 1D and 1E).

During embryonic development, *DUX4* is expressed in a short burst during the cleavage stage (Hendrickson et al., 2017). Re-analysis of human embryo RNA sequencing (RNA-seq) data (Hendrickson et al., 2017) revealed that expression of *H3.X* and *H3.Y* coincided with *DUX4* expression (Figure 1F). Together, these data identify *H3.X* and *H3.Y* as genes regulated by DUX4 and show that they are co-expressed with endogenous *DUX4* in biologically relevant contexts, i.e., FSHD muscle cells and the cleavage-stage human embryo. In addition, we have previously shown *DUX4* expression in the testis (Snider et al., 2010), where *H3.X/Y* expression has also been reported (Wiedemann et al., 2010).

H3.X/Y Are Incorporated in Expressed Regions of the Genome

Previous studies demonstrated that exogenously expressed H3.Y was incorporated into nucleosomal DNA by the HIRA chaperone complex (Zink et al., 2017) at the TSSs of highly expressed genes (Kujirai et al., 2016; Zink et al., 2017). To determine the incorporation pattern of endogenous H3.X/Y in DUX4-expressing cells, we induced *DUX4* in MB135iDUX4 myoblasts and used the antibody-targeted micrococcal nuclease (MNase) CUT&RUN assay (Skene et al., 2018; Skene and Henikoff, 2017) to map H3.X/Y incorporation genome-wide (schematic in Figure 2A). H3.X/Y localized in domains ranging from 500 bp to nearly 100 kb (Figure S2A), with ~75% of domains overlapping genic regions and the remaining 25% intergenic (Figure 2B), similar to what was seen in a previous study using ChIP-seq of tagged H3.Y expressed in HeLa cells (Zink et al., 2017).

H3.X/Y were preferentially incorporated at highly expressed genes (Figure 2C) and at DUX4-induced target genes (Figure 2D). Similarly, 80% of intergenic DUX4-induced long non-coding RNAs (lncRNAs, n = 380) showed H3.X/Y incorporation, and the presence of an intergenic H3.X/Y domain correlated with induction by DUX4 as compared to random intergenic bins of comparable length (Figure 2E). Specific examples of DUX4-induced genes and constitutively expressed genes are shown in Figures 2F and 2G, respectively. Averaging over larger sets of genes showed greater H3.X/Y enrichment at the TSSs of constitutively expressed genes (Figure 2H, left), consistent with previous reports (Kujirai et al., 2016; Zink et al., 2017), whereas H3.X/Y were enriched throughout the entire transcribed region of DUX4-induced genes (Figure 2H, right).

A Pulse of DUX4 Activates Target Gene Expression with Little Cell Toxicity

Mis-expression of *DUX4* induces apoptotic cell death in nearly every cell type tested (Kowaljow et al., 2007; Rickard et al., 2015; Wallace et al., 2011), yet DUX4 is expressed in the germline and early embryo (Hendrickson et al., 2017; Snider et al., 2010), and the Dux mouse ortholog was shown to be important for early embryo development (De Iaco et al., 2017). Unlike in cell culture models, where toxicity occurs with continuous *DUX4* expression, *DUX4* is only briefly expressed in the early embryo. To test whether cells might survive transient expression of DUX4, we treated MB135iDUX4 myoblasts with a 4- to 6-h "pulse" of doxycycline to induce transient *DUX4* expression. In contrast to the continuous expression of *DUX4* that resulted in the death of nearly the entire cell population by 48–72 h, a 4-h pulse of doxycycline resulted in only a small reduction of the cell population at 24 h followed by expansion of that population through the 72-h time point (Figure 3A). Immunodetection showed that a short pulse of doxycycline induced DUX4 expression in nearly all nuclei (Figure 3B). Western analysis confirmed that DUX4 protein and DUX4 targets ZSCAN4 and H3.X/Y/Z were detectable at similar time points as observed for continuous DUX4 expression and persisted for at least 24 h (Figure 3C; compare to Figure 1B). Remarkably, the H3.X and H3.Y proteins remained detectable even 4 days after the initial pulse (Figure 3D). Based on RNA-seq analysis, the transcriptome 24 h after a pulse of *DUX4* largely recapitulated the transcriptional changes characterized by the continuous expression of *DUX4* seen in Jagannathan et al. (2016); $R^2 = 0.63$; Figure 3E. Of the 941 genes that increased by a log2 fold-change > 2.0 (adjusted $p < 0.05$) in the continuous sample, 673 (72%) showed greater than a two-fold change (log2 fold-change > 1.0) 24 h after beginning a 4-h pulse of *DUX4* (Table S1 and red dots in Figure 3E). These results suggest that the duration of *DUX4* expression might be a major determinant of toxicity rather than the cell type and that a brief pulse of DUX4 results in robust activation of its transcriptional program and prolonged presence of H3.X/Y proteins.

H3.X/Y Incorporation Increases the Perdurance and Re-expression of DUX4 Target Genes

To determine whether H3.X/Y incorporation at DUX4 target genes could increase perdurance of gene expression and/or facilitate subsequent gene expression, we induced a pulse of *DUX4* followed by a second pulse 2 days later, when H3.X/Y are present in chromatin (Figure 4A). We compared gene expression with or without H3.X/Y by using small interfering RNAs (siRNAs) that targeted both *H3.X* and *H3.Y* (siXY) or control siRNA (siControl; Figures 4A–4D). RNA for the DUX4 targets *ZSCAN4* and *TRIM43*, both of which overlap with H3.X/Y incorporation (see Figure 2F), were robustly induced 24 h after the first pulse of *DUX4* expression with decreased levels by 48 h after the pulse. A second pulse of *DUX4* 2 days after the first pulse invoked a super-induction of *ZSCAN4* and *TRIM43* 24 h later (day 3), with RNA levels roughly six-fold greater than after the single pulse. Despite similar, or slightly higher, levels of *DUX4* expression (Figure 4B), *H3.X/Y* knockdown prevented this super-induction after the second pulse (Figure 4C). Following either the first pulse or second

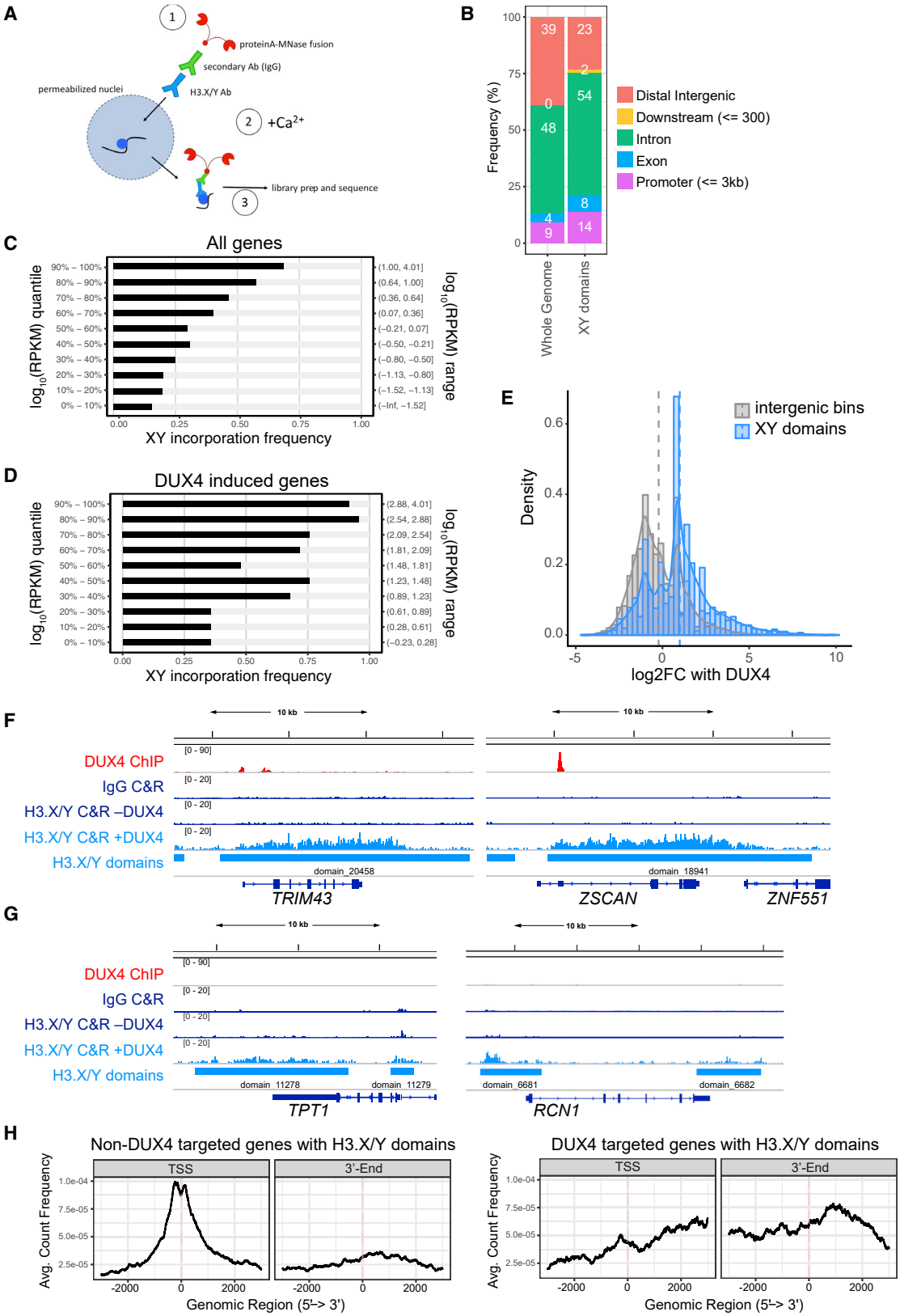

(legend on next page)

pulse of *DUX4*, *ZSCAN4* and *TRIM43* had greater perdurance of expression in siControl-treated cells compared to siXY-treated cells based on both the amount of RNA and the slope of the decline of mRNA (Figure 4D). This suggests that incorporation of H3.X/Y facilitated the increased inducibility of these genes and the persistence of their RNA expression. In contrast to these DUX4 target genes, constitutively expressed genes that incorporated H3.X/Y, e.g., *TPT1* and *XRCC5*, were unaffected by H3.X/Y knockdown (Figures S2B and S2C). Overexpression of FLAG-tagged H3.X or H3.Y in the absence of DUX4 did not induce DUX4 target gene expression (Figures S3A–S3C), indicating that H3.X/Y were enhancing the response to DUX4 rather than acting alone to induce a transcriptional response. Similar to the results in myoblasts, H3.X/Y expression was necessary for enhanced induction of DUX4 target genes following a second pulse of DUX4 in differentiated muscle cells (Figures S4A and S4B), consistent with replication-independent nucleosome incorporation mediated by the HIRA chaperone. Furthermore, H3.X/Y knockdown in FSHD1 and FSHD2 myoblasts or myotubes decreased both DUX4 expression and DUX4 target gene expression (Figures S4C–S4E).

Expanding these experiments genome-wide, we performed RNA-seq 24 h after the 1-pulse and 2-pulse time points for the conditions shown in Figure 4A. Differential gene expression analysis revealed that H3.X/Y were necessary to sensitize nearly all DUX4-induced genes for subsequent super-induction. A single pulse of *DUX4* showed induction of target genes (Figure 4Ei) that were not affected by *H3.X/Y* knockdown (Figure 4Eii), whereas super-induction of DUX4 target genes with a second pulse (Figure 4Eiii) was prevented by *H3.X/Y* knockdown (Figure 4Eiv). In contrast, constitutively expressed non-DUX4 targets with H3.X/Y incorporation were unaffected by pulses of *DUX4* and knockdown treatments (Figure 4F). These results demonstrate that H3.X and H3.Y were incorporated into DUX4-induced genes and that this enhanced future expression of these genes.

DISCUSSION

Together, our data demonstrate that *H3.X* and *H3.Y* are induced by DUX4 in human muscle cells, are induced coincident with *DUX4* expression in human embryos and in FSHD muscle cells, are incorporated at genes induced by DUX4, and that their incorporation both promotes the perdurance of DUX4 target gene expression and facilitates their subsequent induction. Previously, other groups have described important biochemical properties of H3.X and H3.Y, mostly through *in vitro* and mis-expression studies (Kujirai et al., 2016, 2017; Wiedemann et al., 2010; Zink et al., 2017). In particular, the *in vitro* biochemical studies predicting a more relaxed chromatin state with less efficient H1 binding (Kujirai et al., 2016) are consistent with our studies in a DUX4-inducible myoblast cell line showing enhanced transcription of genes incorporating H3.X/Y. In this way, our study builds on these important advances and characterizes biological consequences of endogenous H3.X/Y expression. Future studies will be needed to determine the role of H3.X/Y incorporation during embryogenesis and whether H3.X/Y contribute to FSHD pathophysiology.

In contrast to DUX4 target genes, constitutively expressed genes were mostly unaffected by incorporation of H3.X/Y. This was also associated with a different pattern of incorporation. Whereas H3.X/Y were incorporated throughout the gene body of DUX4 target genes, incorporation at constitutively expressed genes was largely flanking the TSSs, as was previously reported in studies that mis-expressed H3.Y in HeLa cells (Kujirai et al., 2016; Zink et al., 2017). It is possible that this different pattern of incorporation represents the difference between a constitutively expressed gene and an induced but previously silent gene. Because the majority of genes robustly regulated by DUX4 are not expressed in myoblasts, their nucleosomes would likely have canonical H3 histones that would be replaced with H3.X/Y and H3.3 when actively transcribed. In contrast, constitutively expressed genes would already have replaced canonical H3 histones with H3.3 and there might be less turnover in the gene body compared to newly induced genes, restricting H3.X/Y incorporation to nucleosomes flanking the TSS that undergo more rapid turnover. Although speculative, this difference might account for the specificity of perdurance and hyper-induction at DUX4-induced genes that incorporate H3.X/Y.

Another important finding of our study is that skeletal muscle cells survive the DUX4-induced transcriptional program following a transient burst of *DUX4* expression. Using a well-characterized cell culture model (Jagannathan et al., 2016) with

Figure 2. H3.X/Y Are Incorporated in Expressed Regions of the Genome

(A) Schematic of CUT&RUN protocol. H3.X/Y nucleosome is represented by a blue circle. CUT&RUN has been used successfully with antibodies that do not perform well in standard chromatin immunoprecipitation (ChIP) assays (Liu et al., 2018), and we used it for this study because the antibody to H3.X/Y did not work for standard ChIP.

(B) Distribution of genomic annotations containing H3.X/Y domains.

(C) Bar graph depicting association of XY incorporation and all DUX4-induced genes (Jagannathan et al., 2016). Gene expression quantiles (log_10 RPKM quantile; y axis) are plotted against the percentage of genes in each quantile interval overlapping with H3.X/Y domains (x axis). Pearson correlation = 0.958.

(D) Same as (C) for robust DUX4 target genes (n = 251 with adjusted $p < 0.05$, corresponding to H_0: $|lfc| < 4$). Pearson correlation = 0.976.

(E) Histogram of intergenic region expression change with *DUX4* induction. Comparing intergenic H3.X/Y domains with random intergenic bins of comparable size shows an association between H3.X/Y domains and DUX4-induced transcription. Vertical dashed lines mark mean log2 fold change with DUX4 for each group.

(F) DUX4 ChIP-seq (Geng et al., 2012), immunoglobulin G (IgG), or H3.X/Y CUT&RUN (C&R) and called H3.X/Y domains at DUX4 target genes *TRIM43* and *ZSCAN4*.

(G) Same as (F) but for genes constitutively expressed (*TPT* and *RCN1*).

(H) Analysis of the distribution of H3.X/Y CUT&RUN reads within genes. Left panel shows highly expressed, non-DUX4 target genes with H3.X/Y domains (n = 679); right panel shows DUX4 target genes only (n = 191).

See also Figure S2.

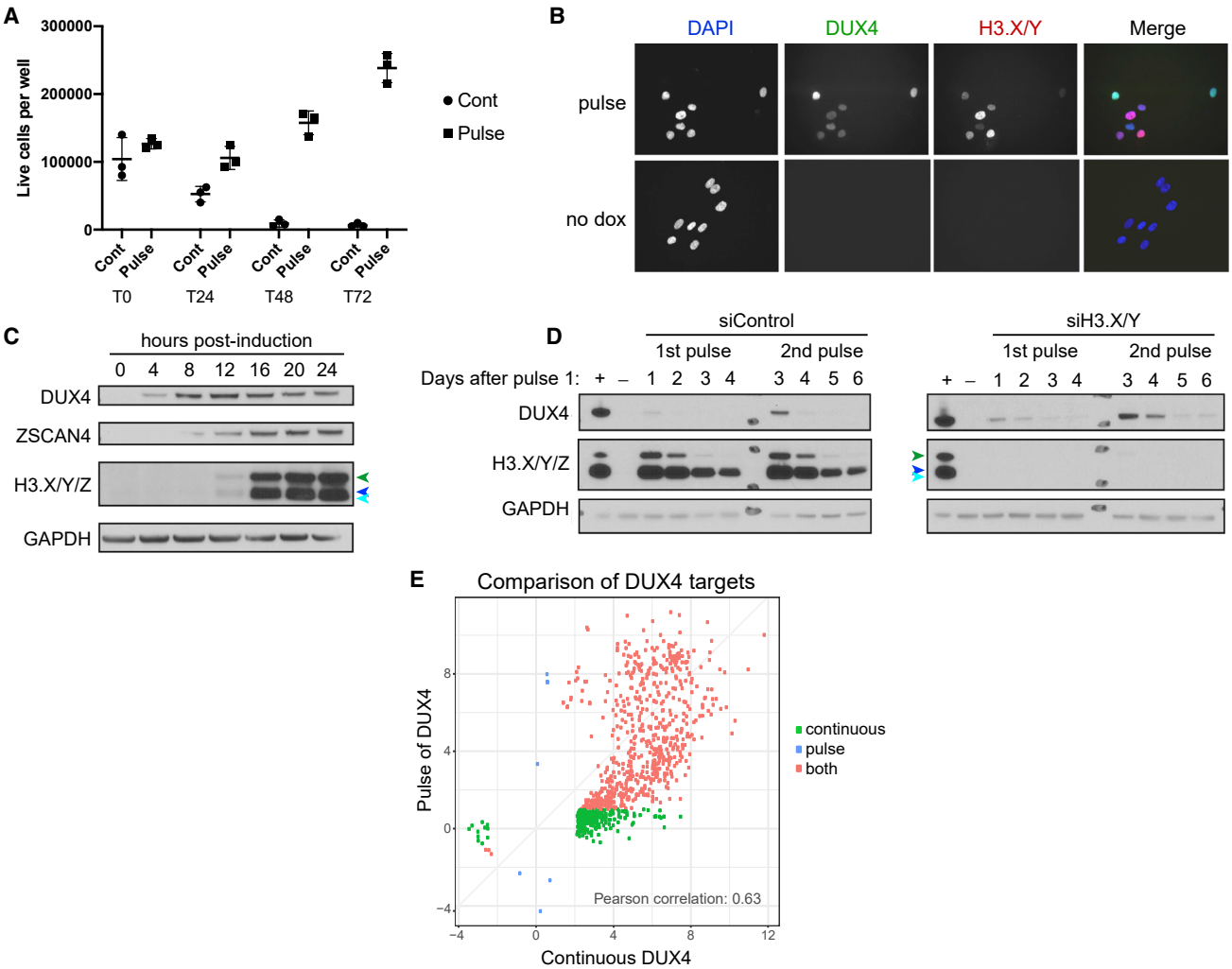

Figure 3. A Pulse of *DUX4* Activates Target Gene Expression with Little Cell Toxicity

(A) Counts of live MB135iDUX4 cells (cells that exclude trypan blue) before and at daily time points after continuous exposure to doxycycline (cont) or a 4-h pulse of doxycycline (pulse). T0, T24, T48, and T72 indicate the hours following initial doxycycline addition.

(B) DUX4 and H3.X/Y immunofluorescence in MB135iDUX4 cells 8 h after the start of a 4-h pulse of doxycycline (pulse) shows induction in nearly all cells, with no staining in uninduced (no dox) cells.

(C) Western blot analysis of MB135iDUX4 cells up to 24 h after *DUX4* pulse. Cells were induced from 0 to 4 h. H3.X/Y/Z are identified with colored arrowheads: H3.Z (green); H3.X (dark blue); and H3.Y (light blue).

(D) MB135iDUX4 cells with control or *H3.X/Y* knockdown with 1 or 2 pulses of *DUX4* on days 0 and 2, respectively, and harvested 1–4 days after each pulse (days 1–4 for 1st pulse; days 3–6 for 2nd pulse). +, continuous dox overnight; –, uninduced day 0 cells. H3.X/Y/Z are identified as in (C).

(E) Comparison of DUX4-induced genes from RNA-seq datasets in MB135iDUX4 cells after continuous (from Jagannathan et al., 2016) or pulsed *DUX4* expression (log2-fold change over no *DUX4* induction with adjusted $p < 0.05$). Axes show degree of gene induction (log2-fold change over no *DUX4*) with adjusted $p < 0.05$ corresponding to H_0: |log2-fold change| < 2. Green indicates genes activated less than 2-fold (log2-fold change < 1.0) in the pulse condition, red indicates genes induced more than 2-fold in the pulse, and blue indicates genes induced by the pulse but less than 2-fold in the continuous.

inducible *DUX4*, it was possible to mimic the kinetics of embryonic *DUX4* expression with short pulses, leading to expression of targets, including *H3.X/Y*, without inducing cell death. This made it feasible to study the effects of *DUX4* expression over several days. This finding has interesting implications for both stem cell biology and FSHD muscular dystrophy. In stem cell biology, brief expression of *DUX4* similar to that in the early embryo occurs in a subset of embryonic stem cells (ESCs) or induced pluripotent stem cells (iPSCs), where it also induces a transcriptional program similar to the cleavage-cell state (Hendrickson et al., 2017; Whiddon et al., 2017; De Iaco et al., 2017). Therefore, our findings suggest that the difference between the early embryo or ESCs/iPSCs that survive *DUX4* expression and FSHD cells or other somatic cells that die when *DUX4* is constitutively expressed might be the duration of expression rather than a protective factor unique to the early developmental program.

In this regard, skeletal muscle might be particularly susceptible to repeated bursts of *DUX4* expression. As our study has

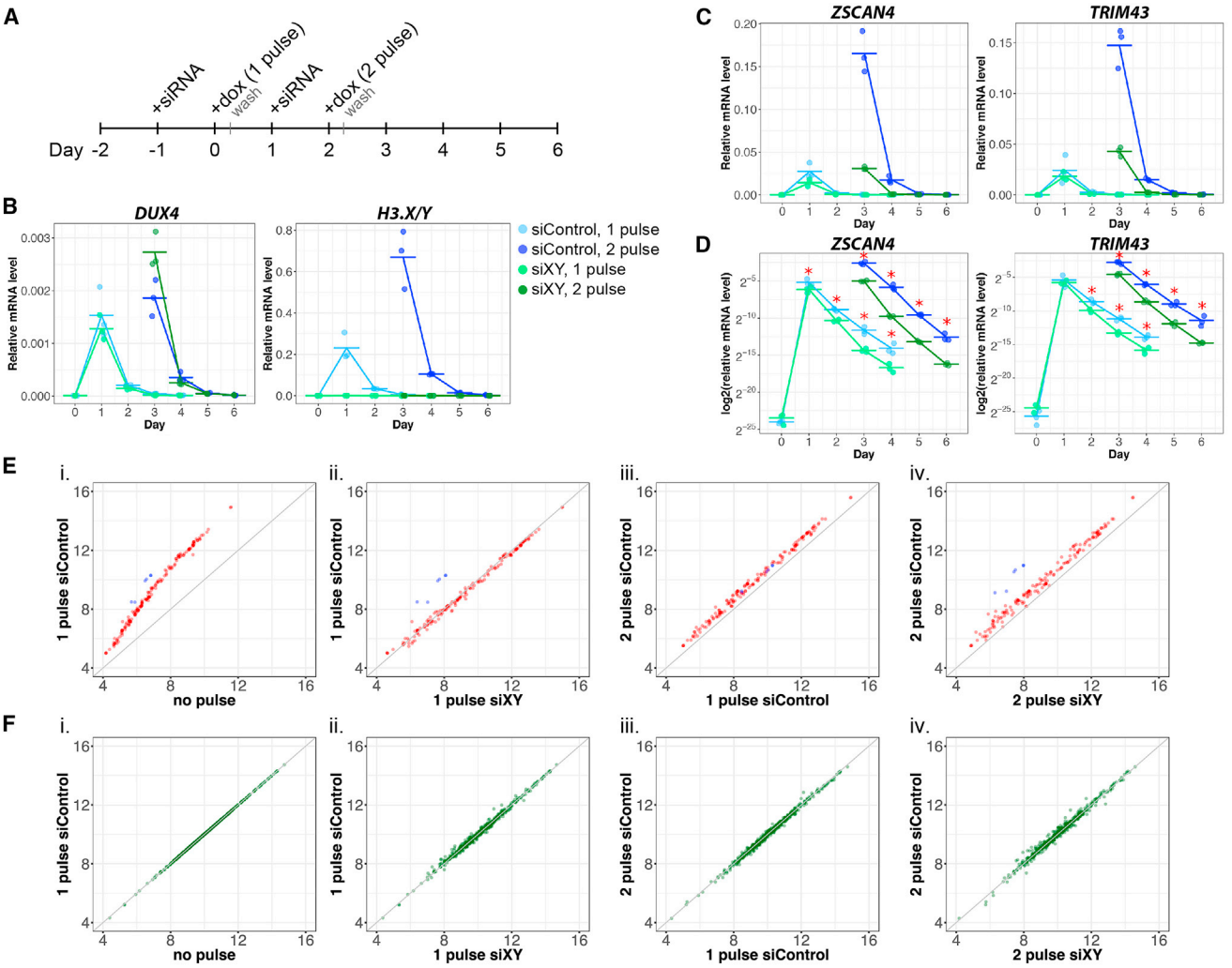

Figure 4. H3.X/Y Incorporation Increases the Perdurance and Re-expression of DUX4 Target Genes

(A) Schematic of experimental design.

(B–D) qRT-PCR in MB135iDUX4 cells with 1 or 2 pulses of *DUX4* and treatment with siH3.X/Y (green) or siControl (blue). Cells were harvested before induction and 1–4 days after each pulse, with 3 biological replicates for each sample shown, relative to *RPL-27*.

(D) Data from (C) plotted on a log scale illustrate differential perdurance of DUX4 target gene expression in siH3.X/Y relative to siControl samples (*$p < 0.05$; one-tailed Wilcoxon rank sum test). Based on a functional t test on the null distribution built by permutations (see STAR Methods), the difference of the slopes between siControl and siH3.XY is significant ($p < 1e{-}12$).

(E) Expression of DUX4 targets measured by RNA-seq in MB135iDUX4 cells, shown as average log2 normalized read counts of biological triplicates. Sequences in the *H3.X/Y* family targeted by siXY are shown in blue. Null model (no difference between conditions) is shown in gray. (1) Induction of *DUX4* targets, (2) comparison of *H3.X/Y* and control knockdown with a single pulse, (3) super-induction of DUX4 targets with a second pulse in control knockdown samples, and (4) knockdown of *H3.X/Y* eliminating super-induction are shown.

(F) Expression of genes with *H3.X/Y* domains that are unaffected by *DUX4*, plotted as in (E).

See also Figures S2 and S4.

demonstrated, incorporation of H3.X/Y in DUX4 target genes increased the perdurance of their expression and enhanced subsequent activation (Figure S4F). Because H3.X/Y use the HIRA chaperone (Kujirai et al., 2016; Zink et al., 2017), they are incorporated into actively transcribed regions independent of DNA replication. As skeletal muscle is post-mitotic and multinucleated, H3.X/Y incorporation could create a prolonged sensitivity for DUX4 target expression, both in the nucleus that initially expressed *DUX4* and in adjacent nuclei that received DUX4 and H3.X/Y from their shared cytoplasm. In this model, stochastic bursts of *DUX4* in different nuclei in a myotube might result in progressive accumulation of H3.X/Y in an expanding nuclear domain and progressive enhancement of expression of DUX4 target genes, resulting in toxicity like that seen with the constitutive expression of *DUX4* (Figure S4G, right). In contrast, incorporation of H3.X/Y following the embryonic burst of *DUX4* would be diluted by subsequent cell divisions (Figure S4G, left). Initially, this could result in greater perdurance of the DUX4-induced

transcriptional program but ultimately not reach toxic levels. It is important to emphasize that these models depict possible biological implications of H3.X/Y function based on data from cell culture studies of DUX4 expression in an engineered cell line and FSHD muscle cells. It will require future studies to verify the details of each model. For example, the burst of DUX4 at the four-cell stage in human embryos is documented (Hendrickson et al., 2017), whereas subsequent bursts of DUX4 in the progeny of these cells has not been described and has yet to be carefully evaluated. Similarly, although H3.X/Y appear to have a role in DUX4 target gene expression in our cell culture models of FSHD, it remains to be shown whether H3.X/Y contribute to FSHD pathophysiology.

STAR★METHODS

Detailed methods are provided in the online version of this paper and include the following:

- KEY RESOURCES TABLE
- LEAD CONTACT AND MATERIALS AVAILABILITY
- EXPERIMENTAL MODEL AND SUBJECT DETAILS
- METHOD DETAILS
  - siRNA treatment
  - CUT&RUN-sequencing
  - RNA isolation and sequencing
  - Western blotting
  - Reverse transcription and qPCR
  - Immunofluorescence
  - Cloning and polyclonal transgenic cell lines
- QUANTIFICATION AND STATISTICAL ANALYSIS
  - Relative quantitation of gene expression
  - CUT&RUN domain calling
  - RNA-seq data analysis of pulsed samples
  - Statistical analysis of qPCR data
  - Software
- DATA AND CODE AVAILABILITY

SUPPLEMENTAL INFORMATION

Supplemental Information can be found online at https://doi.org/10.1016/j.celrep.2019.10.025.

ACKNOWLEDGMENTS

This work was supported by R01AR045203 (S.J.T.), P01NS069539 (S.J.T. and S.M.v.d.M.), Friends of FSH Research (S.J.T.), F31NS101773 (R.R.), T32HG000035 (R.R.), T32HD007183 (R.R.), and T32GM007266 (R.R.). Thank you to Christine Codomo for preparing CUT&RUN libraries and Alyssa Dawson, Elizabeth Jensen, and the rest of the Fred Hutch Genomics Shared Resource for sequencing.

AUTHOR CONTRIBUTIONS

R.R., C.-J.W., D.C.H., and S.J.T. conceived and performed experiments, wrote manuscript, and secured funding. S.B.H., P.J.S., S.H., and S.M.v.d.M. provided reagents, expertise, and feedback.

DECLARATION OF INTERESTS

The authors declare no competing interests.

Received: January 16, 2019
Revised: April 1, 2019
Accepted: October 7, 2019
Published: November 12, 2019

REFERENCES

Ahmad, K., and Henikoff, S. (2002a). Histone H3 variants specify modes of chromatin assembly. Proc. Natl. Acad. Sci. USA *99* (*Suppl 4*), 16477–16484.

Ahmad, K., and Henikoff, S. (2002b). The histone variant H3.3 marks active chromatin by replication-independent nucleosome assembly. Mol. Cell *9*, 1191–1200.

De Iaco, A., Planet, E., Coluccio, A., Verp, S., Duc, J., and Trono, D. (2017). DUX-family transcription factors regulate zygotic genome activation in placental mammals. Nat. Genet. *49*, 941–945.

Drané, P., Ouararhni, K., Depaux, A., Shuaib, M., and Hamiche, A. (2010). The death-associated protein DAXX is a novel histone chaperone involved in the replication-independent deposition of H3.3. Genes Dev. *24*, 1253–1265.

Elsässer, S.J., Noh, K.M., Diaz, N., Allis, C.D., and Banaszynski, L.A. (2015). Histone H3.3 is required for endogenous retroviral element silencing in embryonic stem cells. Nature *522*, 240–244.

Geng, L.N., Tyler, A.E., and Tapscott, S.J. (2011). Immunodetection of Human Double Homeobox 4. HYBRIDOMA *30*, 125–130.

Geng, L.N., Yao, Z., Snider, L., Fong, A.P., Cech, J.N., Young, J.M., van der Maarel, S.M., Ruzzo, W.L., Gentleman, R.C., Tawil, R., and Tapscott, S.J. (2012). DUX4 activates germline genes, retroelements, and immune mediators: implications for facioscapulohumeral dystrophy. Dev. Cell *22*, 38–51.

Goldberg, A.D., Banaszynski, L.A., Noh, K.M., Lewis, P.W., Elsaesser, S.J., Stadler, S., Dewell, S., Law, M., Guo, X., Li, X., et al. (2010). Distinct factors control histone variant H3.3 localization at specific genomic regions. Cell *140*, 678–691.

Hendrickson, P.G., Doráis, J.A., Grow, E.J., Whiddon, J.L., Lim, J.W., Wike, C.L., Weaver, B.D., Pflueger, C., Emery, B.R., Wilcox, A.L., et al. (2017). Conserved roles of mouse DUX and human DUX4 in activating cleavage-stage genes and MERVL/HERVL retrotransposons. Nat. Genet. *49*, 925–934.

Howman, E.V., Fowler, K.J., Newson, A.J., Redward, S., MacDonald, A.C., Kalitsis, P., and Choo, K.H. (2000). Early disruption of centromeric chromatin organization in centromere protein A (Cenpa) null mice. Proc. Natl. Acad. Sci. USA *97*, 1148–1153.

Jagannathan, S., Shadle, S.C., Resnick, R., Snider, L., Tawil, R.N., van der Maarel, S.M., Bradley, R.K., and Tapscott, S.J. (2016). Model systems of DUX4 expression recapitulate the transcriptional profile of FSHD cells. Hum. Mol. Genet. *25*, 4419–4431.

Jones, T.I., Chen, J.C., Rahimov, F., Homma, S., Arashiro, P., Beermann, M.L., King, O.D., Miller, J.B., Kunkel, L.M., Emerson, C.P., Jr., et al. (2012). Facioscapulohumeral muscular dystrophy family studies of DUX4 expression: evidence for disease modifiers and a quantitative model of pathogenesis. Hum. Mol. Genet. *21*, 4419–4430.

Kong, Q., Banaszynski, L.A., Geng, F., Zhang, X., Zhang, J., Zhang, H., O'Neill, C.L., Yan, P., Liu, Z., Shido, K., et al. (2018). Histone variant H3.3-mediated chromatin remodeling is essential for paternal genome activation in mouse preimplantation embryos. J. Biol. Chem. *293*, 3829–3838.

Kowaljow, V., Marcowycz, A., Ansseau, E., Conde, C.B., Sauvage, S., Mattéotti, C., Arias, C., Corona, E.D., Nuñez, N.G., Leo, O., et al. (2007). The DUX4 gene at the FSHD1A locus encodes a pro-apoptotic protein. Neuromuscul. Disord. *17*, 611–623.

Krom, Y.D., Dumonceaux, J., Mamchaoui, K., den Hamer, B., Mariot, V., Negroni, E., Geng, L.N., Martin, N., Tawil, R., Tapscott, S.J., et al. (2012). Generation of isogenic D4Z4 contracted and noncontracted immortal muscle cell clones from a mosaic patient: a cellular model for FSHD. Am. J. Pathol. *181*, 1387–1401.

Kujirai, T., Horikoshi, N., Sato, K., Maehara, K., Machida, S., Osakabe, A., Kimura, H., Ohkawa, Y., and Kurumizaka, H. (2016). Structure and function of human histone H3.Y nucleosome. Nucleic Acids Res. *44*, 6127–6141.

Kujirai, T., Horikoshi, N., Xie, Y., Taguchi, H., and Kurumizaka, H. (2017). Identification of the amino acid residues responsible for stable nucleosome formation by histone H3.Y. Nucleus *8*, 239–248.

Langmead, B., Trapnell, C., Pop, M., and Salzberg, S.L. (2009). Ultrafast and memory-efficient alignment of short DNA sequences to the human genome. Genome Biol. *10*, R25.

Lawrence, M., Huber, W., Pagès, H., Aboyoun, P., Carlson, M., Gentleman, R., Morgan, M.T., and Carey, V.J. (2013). Software for computing and annotating genomic ranges. PLoS Comput. Biol. *9*, e1003118.

Lewis, P.W., Elsaesser, S.J., Noh, K.M., Stadler, S.C., and Allis, C.D. (2010). Daxx is an H3.3-specific histone chaperone and cooperates with ATRX in replication-independent chromatin assembly at telomeres. Proc. Natl. Acad. Sci. USA *107*, 14075–14080.

Liu, N., Hargreaves, V.V., Zhu, Q., Kurland, J.V., Hong, J., Kim, W., Sher, F., Macias-Trevino, C., Rogers, J.M., Kurita, R., et al. (2018). Direct promoter repression by BCL11A controls the fetal to adult hemoglobin switch. Cell *173*, 430–442.e17.

Love, M.I., Huber, W., and Anders, S. (2014). Moderated estimation of fold change and dispersion for RNA-seq data with DESeq2. Genome Biol. *15*, 550.

Lun, A.T., and Smyth, G.K. (2016). csaw: a Bioconductor package for differential binding analysis of ChIP-seq data using sliding windows. Nucleic Acids Res. *44*, e45.

Rickard, A.M., Petek, L.M., and Miller, D.G. (2015). Endogenous DUX4 expression in FSHD myotubes is sufficient to cause cell death and disrupts RNA splicing and cell migration pathways. Hum. Mol. Genet. *24*, 5901–5914.

Robinson, M.D., McCarthy, D.J., and Smyth, G.K. (2010). edgeR: a Bioconductor package for differential expression analysis of digital gene expression data. Bioinformatics *26*, 139–140.

Shadle, S.C., Zhong, J.W., Campbell, A.E., Conerly, M.L., Jagannathan, S., Wong, C.J., Morello, T.D., van der Maarel, S.M., and Tapscott, S.J. (2017). DUX4-induced dsRNA and MYC mRNA stabilization activate apoptotic pathways in human cell models of facioscapulohumeral dystrophy. PLoS Genet. *13*, e1006658.

Skene, P.J., and Henikoff, S. (2017). An efficient targeted nuclease strategy for high-resolution mapping of DNA binding sites. eLife *6*, e21856.

Skene, P.J., Henikoff, J.G., and Henikoff, S. (2018). Targeted in situ genome-wide profiling with high efficiency for low cell numbers. Nat. Protoc. *13*, 1006–1019.

Snider, L., Geng, L.N., Lemmers, R.J., Kyba, M., Ware, C.B., Nelson, A.M., Tawil, R., Filippova, G.N., van der Maarel, S.M., Tapscott, S.J., and Miller, D.G. (2010). Facioscapulohumeral dystrophy: incomplete suppression of a retrotransposed gene. PLoS Genet. *6*, e1001181.

Tachiwana, H., Kagawa, W., Osakabe, A., Kawaguchi, K., Shiga, T., Hayashi-Takanaka, Y., Kimura, H., and Kurumizaka, H. (2010). Structural basis of instability of the nucleosome containing a testis-specific histone variant, human H3T. Proc. Natl. Acad. Sci. USA *107*, 10454–10459.

Tagami, H., Ray-Gallet, D., Almouzni, G., and Nakatani, Y. (2004). Histone H3.1 and H3.3 complexes mediate nucleosome assembly pathways dependent or independent of DNA synthesis. Cell *116*, 51–61.

Tawil, R., van der Maarel, S.M., and Tapscott, S.J. (2014). Facioscapulohumeral dystrophy: the path to consensus on pathophysiology. Skelet. Muscle *4*, 12.

Trapnell, C., Pachter, L., and Salzberg, S. (2009). TopHat: discovering splice junctions with RNA-Seq. Bioinformatics *25*, 1105–1111.

Wallace, L.M., Garwick, S.E., Mei, W., Belayew, A., Coppee, F., Ladner, K.J., Guttridge, D., Yang, J., and Harper, S.Q. (2011). DUX4, a candidate gene for facioscapulohumeral muscular dystrophy, causes p53-dependent myopathy in vivo. Ann. Neurol. *69*, 540–552.

Whiddon, J.L., Langford, A.T., Wong, C.J., Zhong, J.W., and Tapscott, S.J. (2017). Conservation and innovation in the DUX4-family gene network. Nat. Genet. *49*, 935–940.

Wickham, H. (2016). ggplot2: Elegant Graphics for Data Analysis (New York: Springer-Verlag).

Wiedemann, S.M., Mildner, S.N., Bönisch, C., Israel, L., Maiser, A., Matheisl, S., Straub, T., Merkl, R., Leonhardt, H., Kremmer, E., et al. (2010). Identification and characterization of two novel primate-specific histone H3 variants, H3.X and H3.Y. J. Cell Biol. *190*, 777–791.

Yao, Z., Snider, L., Balog, J., Lemmers, R.J., Van Der Maarel, S.M., Tawil, R., and Tapscott, S.J. (2014). DUX4-induced gene expression is the major molecular signature in FSHD skeletal muscle. Hum. Mol. Genet. *23*, 5342–5352.

Yu, G., Wang, L.G., and He, Q.Y. (2015). ChIPseeker: an R/Bioconductor package for ChIP peak annotation, comparison and visualization. Bioinformatics *31*, 2382–2383.

Zerbino, D.R., Achuthan, P., Akanni, W., Amode, M.R., Barrell, D., Bhai, J., Billis, K., Cummins, C., Gall, A., Girón, C.G., et al. (2018). Ensembl 2018. Nucleic Acids Res. *46* (*D1*), D754–D761.

Zink, L.M., Delbarre, E., Eberl, H.C., Keilhauer, E.C., Bönisch, C., Pünzeler, S., Bartkuhn, M., Collas, P., Mann, M., and Hake, S.B. (2017). H3.Y discriminates between HIRA and DAXX chaperone complexes and reveals unexpected insights into human DAXX-H3.3-H4 binding and deposition requirements. Nucleic Acids Res. *45*, 5691–5706.

STAR★METHODS

KEY RESOURCES TABLE

REAGENT or RESOURCE	SOURCE	IDENTIFIER
Antibodies		
GAPDH (6C5)	GeneTex	GTX28245; RRID: AB_37067
DUX4	Geng et al., 2011	E14-3
ZSCAN4	ThermoFisher	PA5-32106; RRID: AB_2549579
H3.X/Y	Wiedemann et al., 2010	clone 8H6-2111; Active Motif Cat# 61161, RRID:AB_2793533
FLAG	Sigma	F3165
Goat anti-rat	Jackson ImmunoResearch	112-035-068
Peroxidase AffiniPure Goat Anti-Rabbit (H+L)	Jackson ImmunoResearch	111-035-144; RRID: AB_2307391
Peroxidase AffiniPure Goat Anti-Mouse IgG (H+L)	Jackson ImmunoResearch	115-035-146; RRID: AB_2307392
Rhodamine (TRITC)-AffiniPure Donkey Anti-Rat IgG	Jackson ImmunoResearch	712-025-150
Fluorescein (FITC)-AffiniPure Donkey Anti-Rabbit IgG	Jackson ImmunoResearch	711-095-152
Rhodamine (TRITC)-AffiniPure Donkey Anti-Mouse IgG	Jackson ImmunoResearch	715-025-151
Bacterial and Virus Strains		
Stbl3 Competent *E. coli*	Generated in-lab	N/A
Chemicals, Peptides, and Recombinant Proteins		
DNase Amp grade	Invitrogen	18068015
RNaseOUT Recombinant Ribonuclease Inhibitor	Invitrogen	10777019
Oligo(dT) 12-18 Primer	Invitrogen	18418012
Superscript III	Invitrogen	18080044
Recombinant human basic fibroblast growth factor	Promega	G5071
Dexamethasone	Sigma-Aldrich	D4902
Puromycin dihydrochloride	Sigma-Aldrich	P833
Blasticidin	GIBCO	R21001
Penicillin/streptomycin	GIBCO	15140122
Doxycycline hyclate	Sigma-Aldrich	D9891
Insulin	Sigma-Aldrich	I1882
Transferrin	Sigma-Aldrich	T-0665
Polybrene	Sigma-Aldrich	107689
Critical Commercial Assays		
Lipofectamine RNAiMAX	Life Technologies	13778150
Lipofectamine 2000	ThermoFisher	11668019
OptiMEM Reduced Serum Medium	ThermoFisher	31985070
iTaq SYBR Green Supermix	Bio-Rad	1725124
NucleoSpin RNA kit	Machery-Nagel	740955
Illumina TruSeq RNA Sample Prep v2 Kit	Illumina	RS-122-2001
Deposited Data		
DUX4 ChIP	Geng et al., 2012; NCBI GEO	GSE33838
continuous DUX4 RNA-seq	Jagannathan et al., 2016; NCBI GEO	GSE85461
early human embryo RNA-seq	Hendrickson et al., 2017; NCBI GEO	GSE72379
RNA-seq data for this study	NCBI Gene Expression Omnibus	GSE119403
CUT&RUN data for this study	NCBI Gene Expression Omnibus	GSE119403
Mendeley Dataset for this study	https://data.mendeley.com/	https://doi.org/10.17632/8mvjj5rw6r.1

(*Continued on next page*)

Continued

REAGENT or RESOURCE	SOURCE	IDENTIFIER
Experimental Models: Cell Lines		
MB135 (female)	Geng et al., 2012	N/A
54-1 (male)	Krom et al., 2012	N/A
MB073 (male, FSHD1)	Fields Center for FSHD and Neuromuscular Research	https://www.urmc.rochester.edu/neurology/fields-center.aspx
54-2 (male, FSHD1)	Krom et al., 2012	N/A
MB200 (male, FSHD2)	Fields Center for FSHD and Neuromuscular Research	https://www.urmc.rochester.edu/neurology/fields-center.aspx
2453 (male, FSHD2)	Fields Center for FSHD and Neuromuscular Research	https://www.urmc.rochester.edu/neurology/fields-center.aspx
MB135iDUX4 (female)	Jagannathan et al., 2016	N/A
MB135iFLAG-H3.3 (female)	This Study	N/A
MB135iFLAG-H3.X (female)	This Study	N/A
MB135iFLAG-H3.Y (female)	This Study	N/A
MB135iH3.Z (female)	This Study	N/A
MB135iGFP (female)	This Study	N/A
Oligonucleotides		
Primers for qPCR and cloning (see Table S2)	This Study	N/A
siRNAs targeting H3.X/Y: UCAAGAAGCCUCACCGCUAUU, GCGGGAAAUCAGAAAGUACUU	This Study (Dharmacon Custom)	N/A
siGENOME non-Targeting #2 Control siRNA	Dharmacon	D-001210-02-20
ON-TARGETplus Non-targeting #1 Control siRNA	Dharmacon	D-001810-01
Recombinant DNA		
pCW57.1	Addgene	41397; RRID: Addgene_41397
pMD2.G	Addgene	12259
psPAX2	Addgene	12260
pCW57.1-FLAG:H3.3	This Study	N/A
pCW57.1-FLAG:H3.X	This Study	N/A
pCW57.1-FLAG:H3.Y	This Study	N/A
pCW57.1-H3.Z	This Study	N/A
pCW57.1-GFP	This Study	N/A
Software and Algorithms		
Bowtie2-2.2.6	Langmead et al., 2009	RRID: SCR_005476; https://github.com/BenLangmead/bowtie/
R package domainCalling	This Study	https://github.com/TapscottLab/domainCalling
ChIPseeker/Bioconductor-3.5	Yu et al., 2015	https://www.bioconductor.org/packages/release/bioc/html/ChIPseeker.html
csaw/Bioconductor-3.5	Lun and Smyth, 2016	https://bioconductor.org/packages/release/bioc/html/csaw.html
Genomic Alignments/Bioconductor-3.5	Lawrence et al., 2013	https://bioconductor.org/packages/release/bioc/html/GenomicAlignments.html
edgeR/Bioconductor-3.5	Robinson et al., 2010	RRID:SCR_012802; http://bioconductor.org/packages/release/bioc/html/edgeR.html/
DESeq2/Bioconductor-3.5	Love et al., 2014	RRID:SCR_000154; http://bioconductor.org/packages/release/bioc/html/DESeq.html
Tophat-2.1.0	Trapnell et al., 2009	RRID:SCR_013035; http://ccb.jhu.edu/software/tophat/index.shtml

(*Continued on next page*)

Continued

REAGENT or RESOURCE	SOURCE	IDENTIFIER
Ensembl v88	Zerbino et al., 2018	RRID:SCR_002344; http://www.ensembl.org//useast.ensembl.org/?redirectsrc=//www.ensembl.org%2F/
CRAN: ggplot2	Wickham, 2016	RRID: SCR_014601; https://cran.r-project.org/web/packages/ggplot2/index.html

LEAD CONTACT AND MATERIALS AVAILABILITY

Further information and requests for resources and reagents should be directed to and will be fulfilled by the Lead Contact, Stephen Tapscott (stapscot@fredhutch.org). In some cases, the Fred Hutchinson Cancer Research Center might require a standard Material Transfer Agreement.

EXPERIMENTAL MODEL AND SUBJECT DETAILS

The following cell lines were used in this study: MB135 (control, female, (Geng et al., 2012), 54-1 (control, male, (Krom et al., 2012), MB073 (FSHD1, male, Fields Center for FSHD and Neuromuscular Research), 54-2 (FSHD1, male, (Krom et al., 2012), MB200 (FSHD2, male, Fields Center for FSHD and Neuromuscular Research), and 2453 (FSHD2, male, Fields Center for FSHD and Neuromuscular Research). FSHD, control, and MB135iDUX4 myoblasts (described in Jagannathan et al., 2016) were grown in F10 growth medium (GIBCO Life Technologies) supplemented with 10% FBS (HyClone), 1% pen/strep (Life Technologies), 10pg/mL fgf (Life Technologies), 1 μM dexamethasone (Sigma), and 2 μg/mL puromycin or 10 μg/mL blasticidin as appropriate to maintain inducibility of the DUX4 transgene. FSHD and control cells were differentiated by growing to confluence and changing to differentiation medium: DMEM (GIBCO) with 1% horse serum (Life Technologies), 1% pen/strep, and 10 μM each transferrin and insulin for 72 h. Pulsed MB135iDUX4 cells were treated with 1 μg/mL doxycycline in growth medium for 6 h for RNA-seq experiments or 4 h for all other experiments, rinsed with PBS, and fresh growth medium added. Cells with continuous induction were treated with 1 μg/mL doxycycline in growth medium overnight or as specified. Differentiated MB135iDUX4 cells were treated with 2μg/mL doxycycline in differentiation medium for 8 h. All cell lines were cultured at 37°C in a humidified incubator supplied with 5% CO_2.

METHOD DETAILS

siRNA treatment

siRNAs for H3.X/Y were designed using the Dharmacon siDESIGN Center. Two siRNAs that gave >90% knockdown were pooled for all experiments to minimize off-target effects with a non-targeting siRNA (Dharmacon D-001210-02-05) used as a control. For pulse experiments, cells were transfected with 50 pg siRNA in OPTIMEM with 7.5 μL Lipofectamine RNAiMax 16 h before each doxycycline treatment. For knockdown experiments in FSHD cells, a double transfection protocol was followed to ensure efficient depletion of pre-existing proteins. FSHD myoblasts were seeded in six-well plates and transfected the next day with 7.5 μL Lipofectamine RNAiMAX and 50pmol of either H3.X/Y-specific siRNA or a non-silencing control siRNA (Dharmacon D-001810-01) diluted in 500 μL OptiMEM Reduced Serum Medium (Thermo Fisher Scientific). Sixteen-hours post-transfection, media was replaced with either supplemented F10 growth media for myoblasts or serum-free differentiation media to promote myotube formation. Forty-eight h following the first transfection, cells were transfected with siRNAs a second time. Fresh media was added 16-hours post-transfection. Cells were harvested for RNA analysis or fixed for immunofluorescence 32 h later.

CUT&RUN-sequencing

MB135iDUX4 cells were treated with or without doxycycline for 18 h before harvesting. Protocol was followed as in Skene et al. (2018) with modifications to scale up for 5 million cells per sample. 100 μL beads were used per sample and wash/incubation volumes were increased to 300-500 μL. 0.05% digitonin was used in the wash buffer. 15 μL H3.X/Y primary antibody (clone 8H6-2111, Active Motif 61161) was used per H3.X/Y sample and incubated for 2 hr. 25 μL rabbit anti-rat secondary (ab6703) was added to each sample for 1 hr. After MNase digestion, fragments were liberated for 20 min and DNA was then purified using the phenol/chloroform method. Three biological replicates were performed for H3.X/Y samples, both with and without doxycycline, and one replicate for each IgG condition.

RNA isolation and sequencing

MB135iDUX4 cells were treated with siRNA knockdown as described above followed by DUX4 pulsing, either once or twice, in triplicate, and harvested 24 h after the start of a pulse. Untreated cells were also harvested from triplicate wells as negative controls. The NucleoSpin RNA kit (Macherey-Nagel) was used to extract RNA from whole cells, following the manufacturer's instructions. RNA-seq

libraries were prepared using the Illumina TruSeq RNA Sample Prep v2 Kit and a PerkinElmer Sciclone NGSx Workstation. All 15 libraries were pooled and sequenced on two flow lanes. The in-house R package and bioinformatics analysis were done with R-3.4.3/Bioconductor-3.5.

Western blotting

Protein was directly lysed from tissue culture plates using 2X Laemlli Buffer with 4% beta mercaptoethanol, sonicated, and boiled for 10 min. Samples were loaded on 4%–12% polyacrylamide gel (Novex) and run with MES buffer, then transferred to a PVDF membrane. Membranes were blocked in 5% milk in PBST for 1 h and incubated with primary antibody in 5% milk overnight at 4° (see KEY RESOURCES TABLE for details on antibodies). After washing, membranes were incubated with appropriate secondary antibodies for 1 h, washed, and detected with chemiluminescence on film.

Reverse transcription and qPCR

RNA was extracted as described for RNA-seq, treated with DNase I (ThermoFisher), and heat inactivated. 500ng-1 μg of RNA was reverse transcribed using SuperScript III First Strand cDNA Synthesis (ThermoFisher) according to manufacturer's instructions, using oligo-dT priming. A no-enzyme sample was also run with a mix of all RNA samples as a control. qPCR was performed using 1x iTaq SYBR Green Master Mix (Bio-Rad) and primers at 1 μM each. Primers listed in Table S2.

Immunofluorescence

Briefly, cells were fixed in 1% formaldehyde for 15 min, permeabilized in PBST, and incubated overnight with primary antibodies. Plates were then washed with PBS, incubated 1 h with fluorescent secondary antibody, counter-stained with DAPI, and imaged using an immersion lens.

Cloning and polyclonal transgenic cell lines

A putative *H3.Z* sequence was identified from RNA-seq reads and used to design primers slightly outside this region. Amplicons from cDNA of *DUX4*-expressing cells were individually subcloned using the TOPO system, miniprepped using the NucleoSpin Plasmid kit (Macherey-Nagel) according to manufacturer's instructions, and Sanger sequenced to generate the final *H3.Z* sequence. FLAG-tagged *H3.X*, FLAG-tagged *H3.Y, H3.Z*, and *GFP* were cloned into pCW57.1 (Addgene #41393). Lentivirus with inducible transgenes were generated by co-transfecting 293T cells with FLAG-tagged H3 variant constructs, pMD2.G (Addgene #12259) and psPAX2 (Addgene #12260) using lipofectamine 2000 (ThermoFisher). To generate polyclonal lines, MB135 cells were transduced with lentivirus. Stable cell lines were selected and maintained in 2 μg/mL puromycin.

QUANTIFICATION AND STATISTICAL ANALYSIS

Relative quantitation of gene expression

Quantitative PCR was carried out on a QuantStudio 7 Flex (Applied Biosystems). Relative expression levels of target genes were normalized to that of reference housekeeping gene *RPL-27* using the relative standard curve method (Figures 4A–4C, S2B, S2C, and S4B) or by using the Comparative Ct Method (ΔΔCt; Figures 1C, S1E, S4D, and S4E). For Figure 1C, samples were normalized to the average of all control replicates, and any samples from control lines that had undetectable signal were set to 0 and not used for normalizing. Information about statistical details can be found in the figure legends. Throughout, graphs represent means with error bars representing standard deviation (SD) of biological triplicate measurements.

CUT&RUN domain calling

Our CUT&RUN data consist of 25 bps long, paired-end reads with average fragment length of 180 bps. We aligned reads to both human genome hg38 and spike-in genome dm6 using Bowtie2-2.2.6 with the following comment: bowtie2–local–very-sensitive-local–no-unal–no-mixed–no-discordant -q–phred33 -I 10 -X 700.

Since H3.X/Y were incorporated in many large regions within gene bodies, conventional peak calling algorithms such as MACS2 were not applicable. We thus developed an in-house R/Bioconductor package *domainCalling* (https://github.com/TapscottLab/domainCalling). The major functionalities of *domainCalling* include spike-in factor normalization and domain (broad peak) detection. To call the domains, the algorithm starts by counting reads overlapping with a sliding window throughout the genome for non-background (DOX+) and background (IgG or DOX-) samples. This window-based counting scheme is implemented by the csaw R/Bioconductor package (Lun and Smyth, 2016). After the counts are normalized by spike-in normalization, it filters out uninteresting windows if the average abundance of the non-background samples is (1) less than three-fold above background or (2) does not exceed the threshold, which is three reads per window. Finally, the retained windows are merged with neighbors within 2kbp distance. H3.X/Y domains were called for merged regions longer than 500 bps.

RNA-seq data analysis of pulsed samples

To preprocess the RNA-seq reads, we filtered out unqualified reads and aligned the reads to human genome hg38 using Tophat-2.1.0. We then profiled the gene expression using features collected from Ensembl v88 and the hit-counting function

summarizeOverlaps() from Bioconductor's GenomicAlignments package. To identify robust DUX4 target genes, we used DESeq2 comparing pulse1 siControl samples to negative controls. The alternative hypothesis is set to $|\beta| > 4$, where β denotes log2 fold change. 170 genes with adjusted p value < 0.05 were determined as robust DUX4 targets.

Statistical analysis of qPCR data

To test the significance of the perdurance effect of H3.X/Y (Figure 4D), we used functional data analysis (https://cran.r-project.org/web/packages/fda/index.html) treating the time course RT-qPCR expression data as a function or graph. The method started with registering the feature of the graph for each treatment, which was the day 1 data where the slope turned from positive to negative. Next it aligned the graphs of two groups of treatments at the value of the feature, and then, for each treatment, constructed a linear combination of functions interpolating the aligned time-course data starting from day 1 to day 4. Finally taken the null distribution built by 250 permutations, we applied the functional t test (fda::*tperm.fd*) to determine the difference between two groups of functions.

Software

The bioinformatics analysis was mostly performed on R-3.4.3/Bioconductor-3.5. The major infrastructure packages used include *csaw*, *edgeR*, *GenomicAlignments*, *ChIPseeker* and *ggplot2*.

DATA AND CODE AVAILABILITY

The MB135iDUX4 pulsed RNA-seq data and CUT&RUN data generated during this study are available at the Gene Expression Omnibus (GEO accession number GSE119403). Other datasets used in this study include DUX4 ChIP-seq (GEO accession number GSE33838), continuous DUX4 RNA-seq (GEO accession number GSE85461), and early embryo RNA-seq (GEO accession number GSE72379). The H3.Z sequence shown in Figure S1A has been submitted to GenBank and is awaiting an accession number. Code availability is detailed in the Key Resources Table with the following references: (Langmead et al., 2009; Lawrence et al., 2013; Love et al., 2014; Robinson et al., 2010; Shadle et al., 2017; Yu et al., 2015; Zerbino et al., 2018).

Cell Reports, Volume *29*

Supplemental Information

DUX4-Induced Histone Variants H3.X and H3.Y Mark DUX4 Target Genes for Expression

Rebecca Resnick, Chao-Jen Wong, Danielle C. Hamm, Sean R. Bennett, Peter J. Skene, Sandra B. Hake, Steven Henikoff, Silvère M. van der Maarel, and Stephen J. Tapscott

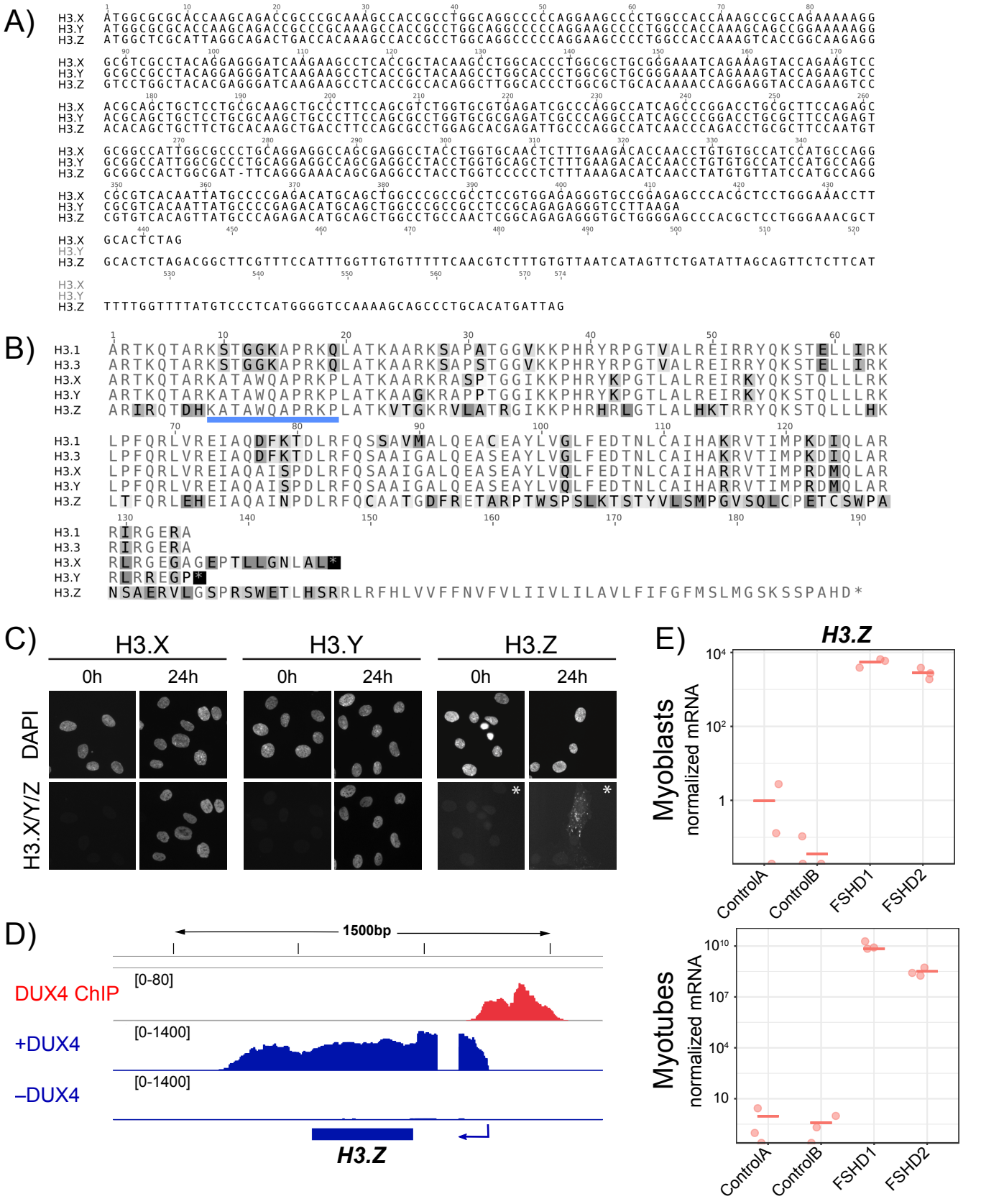

Figure S1. H3.Z is directly induced by DUX4. Related to Figure 1.

A) DNA sequence alignment of H3.X, H3.Y, and H3.Z. H3.Z frameshift is highlighted in blue. B) Protein sequence alignment of H3.1, H3.3, H3.X, H3.Y, and H3.Z. Epitope for H3.X/Y/Z antibody is noted with a blue line. C) Immunofluorescence of H3.X, H3.Y, or H3.Z from a MB135-derived polyclonal cell line with dox-inducible integrated transgenes after 0- or 24-hour doxycycline treatment (*enhanced contrast to detect H3.Z staining). D) RNA-seq reads of MB135iDUX4 cells with and without DUX4 induction (Jagannathan et al., 2016) that align to the H3.Z locus, as well as DUX4 ChIP-seq (Geng et al., 2012) showing a peak upstream of H3.Z. E) RT-qPCR analysis of H3.Z as in Figure 1C.

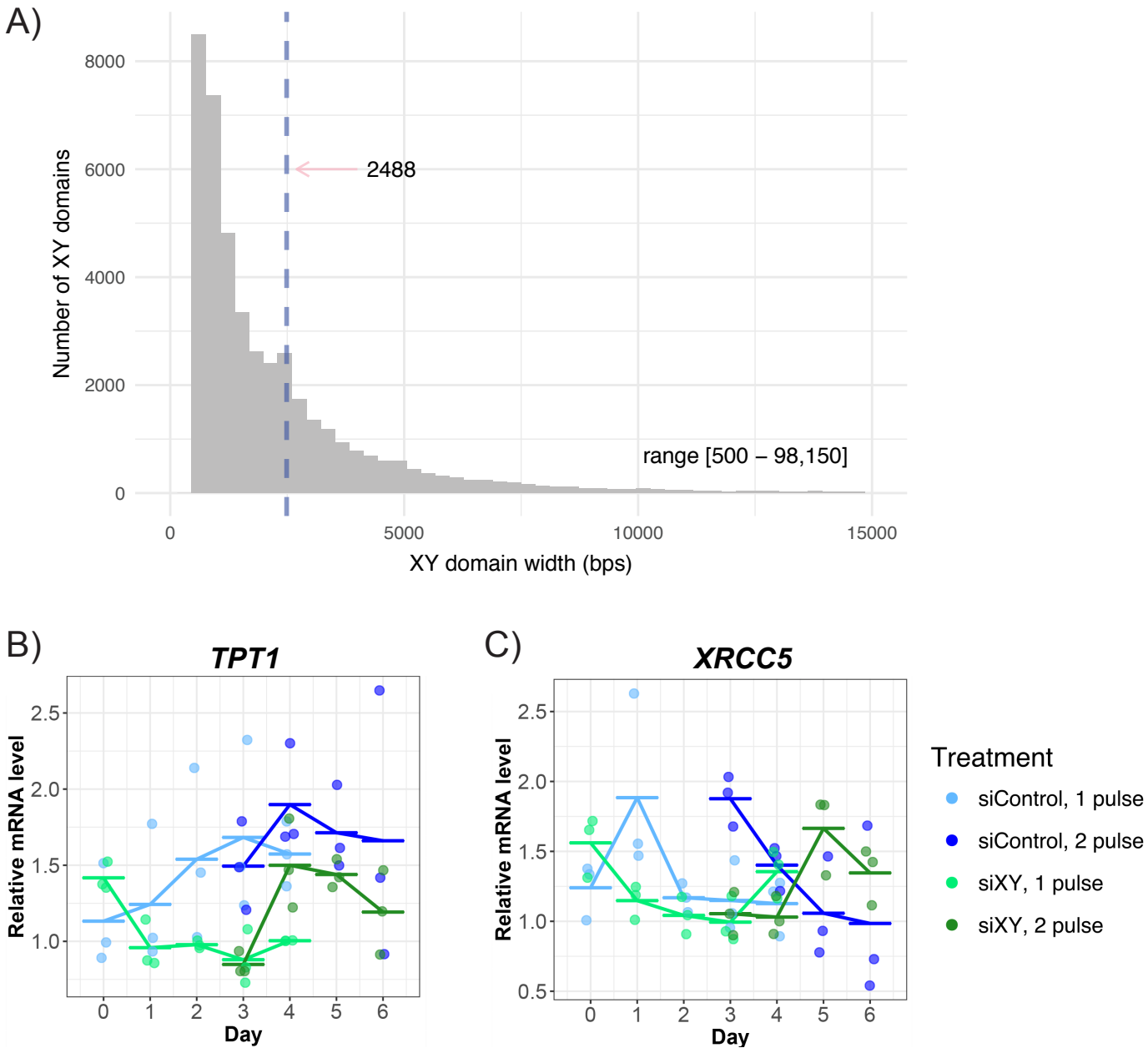

Figure S2. H3.X/Y knockdown does not affect expression of constitutively-expressed genes. Related to Figure 2 and Figure 3.
A) Histogram of H3.X/Y CUT&RUN domain sizes. Mean is marked with a dashed blue line. B,C) RT-qPCR in MB135iDUX4 cells with 1 or 2 pulses of DUX4 and treatment with siH3.X/Y (green) or siControl (blue). Cells were harvested before induction and 1-4 days after each pulse. Data displayed as mean ±S.D. of biological triplicate measurements for each sample shown, relative to *RPL-27*.

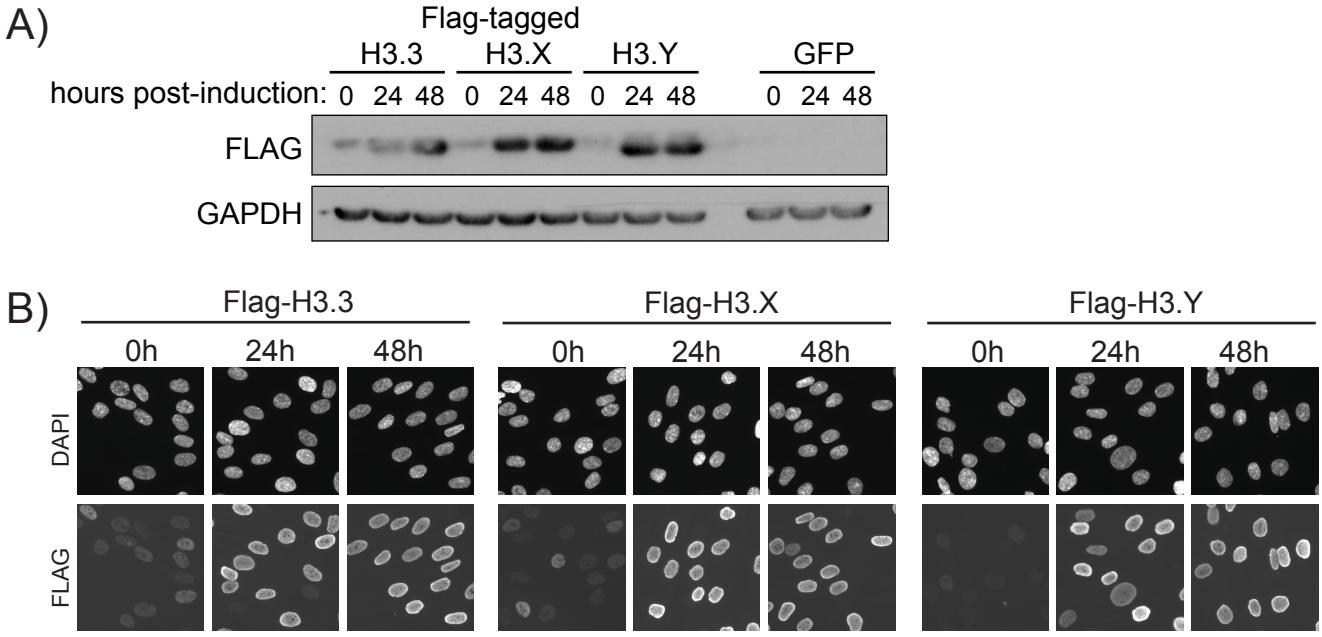

C) transgene

Construct	Induced?	Expressed?	avg CT - dox	avg CT + dox
GFP	++	yes +/- dox	24.4	18.3
flag-H3.3	++	yes +/- dox	21.5	15.0
flag-H3.X	++	yes +/- dox	22.9	15.1
flag-H3.Y	++	yes +/- dox	23.9	15.1

RPL-27

Construct	Induced?	Expressed?	avg CT - dox	avg CT + dox
GFP	-	yes +/- dox	16.4	16.2
flag-H3.3	-	yes +/- dox	16.1	16.1
flag-H3.X	-	yes +/- dox	16.1	16.2
flag-H3.Y	-	yes +/- dox	16.1	16.1

TRIM43

Construct	Induced?	Expressed?	avg CT - dox	avg CT + dox
GFP	-	no	32.1	31.0
flag-H3.3	-	no	30.9	30.7
flag-H3.X	-	no	29.9	31.5
flag-H3.Y	-	no	31.5	30.6

ZSCAN4

Construct	Induced?	Expressed?	avg CT - dox	avg CT + dox
GFP	-	no	29.4	29.9
flag-H3.3	-	no	29.1	29.2
flag-H3.X	-	no	29.5	29.2
flag-H3.Y	-	no	29.5	29.4

Figure S3. H3.X/Y overexpression is not sufficient to induce DUX4 target gene expression. Related to Figure 4.
A) Western blot analysis of MB135-derived polyclonal cell lines with dox-inducible FLAG-tagged H3 variant integrated transgenes after 0-, 24-, and 48-hour doxycycline treatment. B) Immunofluorescence of FLAG-tagged protein expression in transgenic cell lines after 0- or 24-, and 48-hour doxycycline treatment. C) qPCR analysis of FLAG-tagged transgenes, *RPL-27*, and DUX4-target genes (*TRIM43* and *ZSCAN4*) after 0- or 24-hour doxycycline treatment. Values represent the average of biological triplicate measurements.

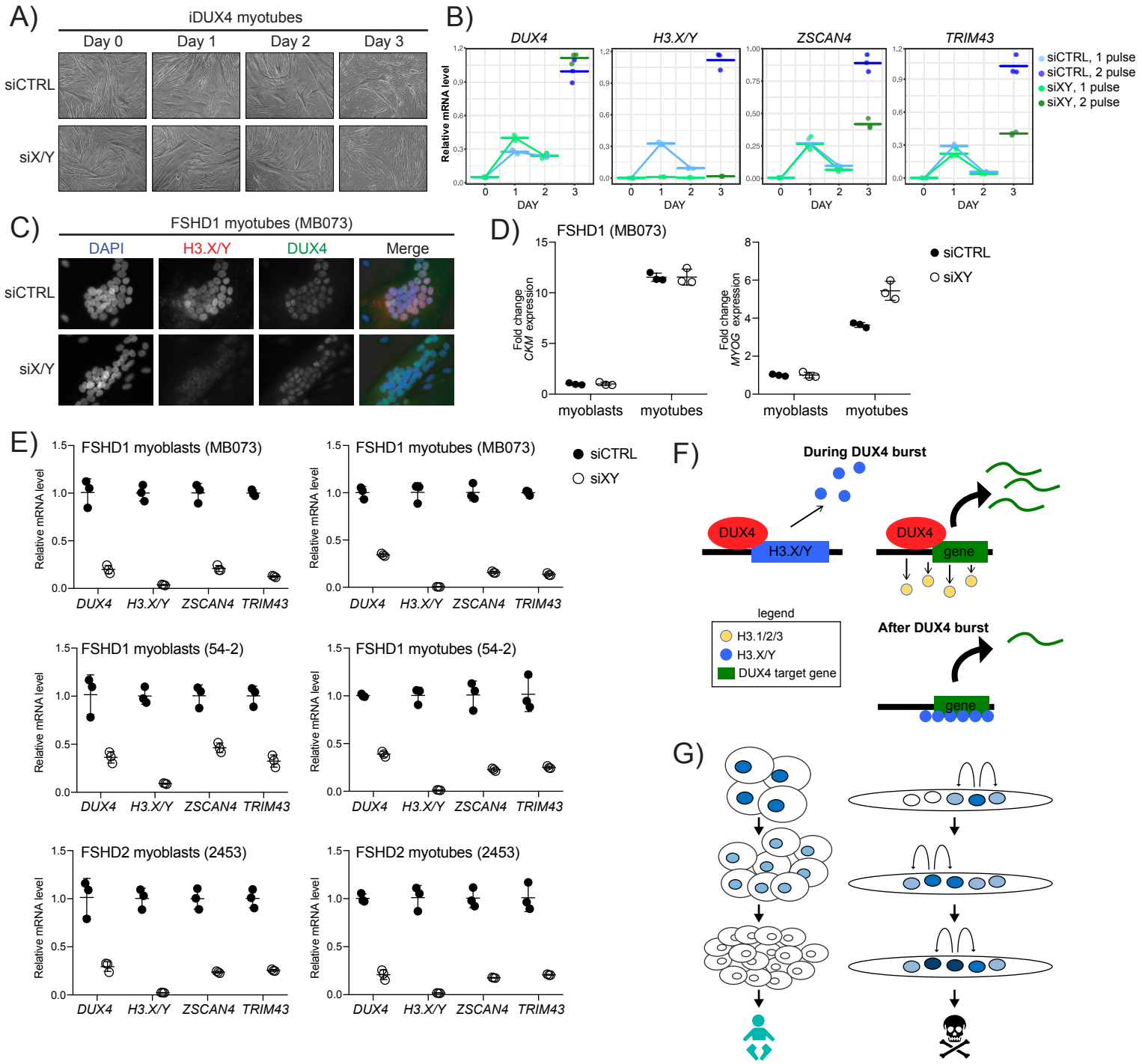

Figure S4. H3.X/Y function in DUX4-expressing differentiated muscle cells. Related to Figure 4.
A) Bright field microscopy images of differentiated MB135iDUX4 muscle cells taken before induction and 24 hours after each pulse. B) RT-qPCR in differentiated MB135iDUX4 cells with 1 or 2 pulses of DUX4 and treatment with siH3.X/Y (green) or siControl (blue). C) Representative immunofluorescence of H3.X/Y (red) and DUX4 (green) in FSHD1 myotubes treated with siControl or siH3.X/Y show sufficient protein knockdown. D) Fold-change expression of myogenic markers *muscle creatine kinase (CKM)* and *myogenin (MYOG)* in differentiated FSHD1 myotubes relative to myoblasts show that H3.X/Y knockdown did not decrease *DUX4* or target gene expression by inhibiting differentiation. E) RT-qPCR analysis of *DUX4* and DUX4-target gene expression following Control or H3.X/Y siRNA-mediated knockdown in three patient-derived immortalized FSHD cell lines (MB073, 54-2, and 2453) for both myoblasts and differentiated myotubes. RT-qPCR data displayed as mean ±S.D. of biological triplicate measurements for each sample shown, relative to *RPL-27*. F) Model of H3.X/Y induction during a DUX4 burst and incorporation into DUX4-regulated genes. G) Incorporation of H3.X/Y (deeper blue denotes more H3.X/Y incorporation) at DUX4-induced genes might contribute to more perdurant DUX4-target expression in the early embryo and to an amplification of DUX4-target expression with successive bursts of DUX4 in different nuclei of a multinucleated muscle (left and right, respectively).